DNA: Replication, Repair, and Recombination:

UvrB Domain 4, an Autoinhibitory Gate for Regulation of DNA Binding and ATPase Activity

Hong Wang, Matthew J. DellaVecchia, Milan Skorvaga, Deborah L. Croteau, Dorothy A. Erie and Bennett Van Houten

J. Biol. Chem. 2006, 281:15227-15237.
doi: 10.1074/jbc.M601476200 originally published online April 4, 2006

THE JOURNAL OF BIOLOGICAL CHEMISTRY VOL. 281, NO. 22, pp. 15227–15237, June 2, 2006
Printed in the U.S.A.

UvrB Domain 4, an Autoinhibitory Gate for Regulation of DNA Binding and ATPase Activity*

Received for publication, February 15, 2006, and in revised form, March 28, 2006 Published, JBC Papers in Press, April 4, 2006, DOI 10.1074/jbc.M601476200

Hong Wang[‡1], Matthew J. DellaVecchia[‡1], Milan Skorvaga[§], Deborah L. Croteau[‡], Dorothy A. Erie[¶], and Bennett Van Houten[‡2]

From the [‡]Laboratory of Molecular Genetics, NIEHS, National Institutes of Health, Department of Health and Human Services, Research Triangle Park, North Carolina 27709, the [§]Department of Molecular Genetics, Cancer Research Institute, Slovak Academy of Sciences, 83391 Bratislava, Slovakia, and the [¶]Department of Chemistry, University of North Carolina, Chapel Hill, North Carolina 27599

UvrB, a central DNA damage recognition protein in bacterial nucleotide excision repair, has weak affinity for DNA, and its ATPase activity is activated by UvrA and damaged DNA. Regulation of DNA binding and ATP hydrolysis by UvrB is poorly understood. Using atomic force microscopy and biochemical assays, we found that truncation of domain 4 of *Bacillus caldotenax* UvrB (UvrBΔ4) leads to multiple changes in protein function. Protein dimerization decreases with an ~8-fold increase of the equilibrium dissociation constant and an increase in DNA binding. Loss of domain 4 causes the DNA binding mode of UvrB to change from dimer to monomer, and affinity increases with the apparent dissociation constants on nondamaged and damaged single-stranded DNA decreasing 22- and 14-fold, respectively. ATPase activity by UvrBΔ4 increases 14- and 9-fold with and without single-stranded DNA, respectively, and UvrBΔ4 supports UvrA-independent damage-specific incision by Cho on a bubble DNA substrate. We propose that other than its previously discovered role in regulating protein-protein interactions, domain 4 is an autoinhibitory domain regulating the DNA binding and ATPase activities of UvrB.

Nucleotide excision repair (NER)[3] is a DNA repair pathway conserved from bacteria to eukaryotes. DNA damage recognition and incision during NER in prokaryotes is a complex process involving UvrA, UvrB, and UvrC (1–3). UvrA and UvrB interact in solution, forming a UvrAB complex (4). It is believed that UvrA, as a dimer within the UvrAB complex, first recognizes helical distortions induced by DNA damage. Upon binding of UvrAB (either as $UvrA_2B$ or $UvrA_2B_2$) to the site of DNA damage (4, 5), conformational changes in the UvrAB-DNA complex lead to transfer of DNA from UvrA to UvrB and dissociation of UvrA (6–10). After dissociation of UvrA from the protein-DNA complex, a very stable UvrB-DNA preincision complex is formed. UvrC recruitment by the UvrB-DNA precincision complex to the site of DNA damage leads to dual incisions on the damaged DNA strand (11–13).

UvrB plays a central role in bacterial NER. In the absence of UvrA, UvrB binds weakly to DNA and has no ATPase activity (2, 14). In the presence of DNA damage, through interaction with UvrA both DNA binding and ATPase activities of UvrB are activated. This allosteric control of UvrB activation is not well understood. UvrB is classified as a member of the helicase superfamily II (15). Crystal structures of the proteins from different organisms (16–18) and most recently the Y96A variant from *Bacillus caldotenax* (19) have shed light on structural components of UvrB. UvrB consists of five domains, namely 1a, 1b, 2, 3, and 4 (16). Even though UvrB contains all the elements of an intact helicase, including all residues implicated in coupling ATP hydrolysis to strand translocation, it is not a true helicase (2, 3, 20). Rather, the limited DNA unwinding activity of UvrAB complex is believed to be important in destabilizing duplex DNA and creating an "entry site" for UvrB to form a stable UvrB-DNA preincision complex (2, 20, 21). A unique structural element in UvrB is a flexible β-hairpin that extrudes from domain 1a, near the wall of domain 1b. Based on superposition of the UvrB structure with known structures of UvrB-related helicase-DNA complexes, a padlock model for the UvrB-DNA preincision complex was proposed (16, 22). In this model, the β-hairpin bifurcates the duplex DNA, and one of the single strands is locked between the β-hairpin and domain 1b. This model was recently confirmed by a UvrB-DNA co-crystal structure (49). The C-terminal domain 4 of UvrB is not visible in any of the available full-length UvrB crystal structures. However, crystallography and NMR spectroscopy studies of the C-terminal fragment of *E. coli* UvrB have revealed that the last 46 amino acids of domain 4 adapt a coiled-coil structure and dimerize through specific hydrophobic and ionic interactions (23, 24). Previously, it has been demonstrated that domain 4 is involved in interacting with UvrC and promoting dimer formation of UvrB (5, 13, 25).

In this study, we provide quantitative measurement of the effect of domain 4 on UvrB self-association, and demonstrate that domain 4 functions as an autoinhibitory domain. Autoinhibitory domains are regions that negatively regulate the activity of a second, separable domain and can provide tight "on site" repression that restrains the targeted domain in a secure off state (26). Autoinhibition is a general method for achieving a high level of specificity and tight regulation in DNA binding site selection (26). Specifically, we show that truncation of domain 4 (residues Pro^{612} to Gly^{658}) of UvrB leads to: 1) a change in UvrB DNA binding mode and increase in DNA binding affinity; 2) an increase in UvrB ATPase activity; and 3) UvrA-independent, damage-specific incision of a bubble substrate mediated by Cho (UvrC homolog). These data suggest that DNA repair enzymes may represent another important class of DNA-binding proteins that are regulated by autoinhibitory domains.

* This work was supported by the Intramural Research Program of the NIEHS, National Institutes of Health. The costs of publication of this article were defrayed in part by the payment of page charges. This article must therefore be hereby marked "*advertisement*" in accordance with 18 U.S.C. Section 1734 solely to indicate this fact.

[1] Both authors contributed equally to this paper.

[2] To whom correspondence should be addressed: NIEHS, 111 Alexander Dr., P. O. Box 12233, Research Triangle Park, NC 27709. Tel.: 919-541-7752; Fax: 919-541-7593; E-mail: vanhout1@niehs.nih.gov.

[3] The abbreviations used are: NER, nucleotide excision repair; WT, wild type; EMSA, electrophoresis mobility shift assay; BisTris, 2-[bis(2-hydroxyethyl)amino]-2-(hydroxymethyl)propane-1,3-diol; AMPPNP, 5′-adenylyl-β,γ-imidodiphosphate; MOPS, 4-morpholinepropanesulfonic acid; ssDNA, single-stranded DNA; dsDNA, double-stranded DNA; AFM, atomic force microscopy.

MATERIALS AND METHODS

Cloning, Expression, and Purification of B. caldotenax UvrA, UvrB, and Escherichia coli Cho Proteins—Genes encoding *B. caldotenax* UvrA, UvrB, and *E. coli* Cho were subcloned in the pTYB1 vector of the T7 IMPACT system (New England Biolabs). The domain 4 truncation mutation of *B. caldotenax* UvrB (UvrBΔ4, sequence between Pro^{612} to Gly^{658} deleted) was constructed following the protocol of the QuikChange site-directed mutagenesis kit (Stratagene). The presence of the desired deletion and absence of additional mutations in the entire amplified *uvrB* gene were confirmed by DNA sequencing. Domain 2 deletion of *B. caldotenax* UvrB (UvrBΔ2, sequence between Leu^{157} and Pro^{245} deleted) was constructed as described previously (19). UvrA and UvrB proteins were expressed in Rosetta-gami(DE3)pLacI (Merck Biosciences) and BL21-CodonPlus®(DE3)-RIL (Stratagene) cells, respectively. Mutant UvrB proteins were expressed following the same procedures used for wild type (WT). All proteins were purified using the IMPACT™-CN system (New England Biolabs) as described previously (16). For purification of Cho, pooled material after elution from a chitin-binding column was purified further over a Superdex 200 HR 10/30 column (GE Healthcare) equilibrated with column buffer (20 mM Tris-HCl, pH 8.0, 500 mM NaCl, 10 mM $MgCl_2$). Proteins used in this study are more than 95% pure as judged by staining of SDS-PAGE protein gel with SimplyBlue™ SafeStain (Invitrogen).

DNA Substrates—DNA substrates were synthesized by Sigma Genosys and 5′ labeled using OptiKinase (U. S. Biochemical Corp.) and [γ-^{32}P]ATP (10 μCi/μl, GE Healthcare) or 3′ labeled using terminal transferase (Roche Applied Science) and [α-^{32}P]ATP (10 μCi/μl, GE Healthcare) according to the manufacturers' instructions. Reactions were terminated with 20 mM EDTA and heat denaturation (65 °C, 10 min). Free nucleotides were subsequently removed by gel filtration chromatography (Micro Biospin-6, Bio-Rad). Fully duplexed DNA (F50/NDB50) and bubble DNA (F50/B8) were constructed by annealing labeled F50 (4 pmol) with equal molar amounts of their respective "bottom" strands. Double-stranded character and homogeneity of the annealed DNA were examined on a 10% native polyacrylamide gel. The 5′ end-labeled duplex DNA containing the UV-activated arylazido cross-linker moiety, $XL2_{25}$, was prepared as described previously (10). The DNA substrate (HS1F-M13mp19) used for the strand-destabilizing assays was labeled and constructed as described previously (27).

Atomic Force Microscopy—Proteins were diluted in buffer (50 mM Tris-HCl, pH 7.5, 100 mM KCl, 10 mM $MgCl_2$) and heated (65 °C, 10 min). Afterward, samples were deposited onto freshly cleaved ruby mica (Spruce Pine Mica Company) pre-warmed to 55 °C on a hot plate. Sample preparation and image collection using Nanoscope III (Veeco Instruments) operated in tapping mode in air were done as described previously (28). The atomic force microscopy (AFM)-derived volume for each protein was obtained as described previously (29). The standard equation employed for converting AFM volume (nm^3) to molecular mass (M_r) is given by the following equation (30).

$$M_r = \frac{\text{AFM volume} + 14.7}{1.2} \qquad \text{(Eq. 1)}$$

Electrophoresis Mobility Shift Assay (EMSA)—Proteins and ssDNA substrates were preheated (65 °C, 10 min) prior to mixing. For single-stranded DNA (ssDNA), UvrB (WT or Δ4) was incubated with 1 nM DNA substrate (5′-^{32}P-labeled) in 20 μl of reaction buffer (50 mM Tris-HCl (pH 7.5), 50 mM KCl, 5 mM dithiothreitol) at 55 °C for 30 min. Half of the reaction was removed immediately after incubation and loaded onto an 8% native polyacrylamide gel (29:1). Gels were run (100 V, 4 h, 4 °C) in 1× TBE buffer (89 mM Tris, 89 mM boric acid, 2.5 mM EDTA). For bubble DNA, the procedures are the same except that the reactions were done in 1× ABC buffer (50 mM Tris-HCl, pH 7.5, 50 mM KCl, 10 mM $MgCl_2$, 1 mM ATP, and 5 mM dithiothreitol) containing 7 μg/ml bovine serum albumin. Reactions were loaded onto a 6 or 8% native polyacrylamide gel (29:1) containing 0.5× TBE, 10 mM $MgCl_2$, and 1 mM ATP. Gels were run (100 V, 2 h, 4 °C) in buffer containing 0.5× TBE, 10 mM $MgCl_2$, and 1 mM ATP. All gels were dried and exposed to a PhosphorImager screen (GE Healthcare) overnight. The B1- and B2-DNA complexes were resolved as distinct peaks and quantified using ImageQuant software (GE Healthcare). The concentration of protein dimer and monomer in each reaction was determined as described in Table 2. The apparent dissociation constants of B2-DNA for WT UvrB and B1-DNA complex for UvrBΔ4 were determined by nonlinear regression analysis (Table 2) (31).

UvrA- and UvrB-DNA Cross-linking Assay—DNA (2 nM, $XL2_{25}$) was incubated with 200 nM UvrA or 5 μM UvrB (WT or Δ4) (55 °C, 15 min, dark) in 20 μl containing: 50 mM Tris-HCl (pH 7.5), 150 mM KCl, 10 mM $MgCl_2$, 0.1 mg/ml bovine serum albumin, and 1 mM ATP (Roche), GTP (Roche), or AMPPNP (Sigma). Reactions were irradiated for 5 min on a platform 5 cm below a 365-nm UV lamp (UVP, Blak-Ray Longwave UV Mercury lamp, 100 watts). NuPage (Invitrogen) 4× lithium dodecyl sulfate (LDS) sample buffer (8 μl) containing dithiothreitol was added to 12 μl of the reaction and heated (85 °C, 15 min). Cross-linked products were resolved on a 10% NuPage BisTris gel in 1× NuPage MOPS SDS running buffer. Gels were dried, developed via PhosphorImager, and quantified using ImageQuant software (GE Healthcare).

ATP/GTP Hydrolysis Assay—Hydrolysis of ATP or GTP by UvrAB was monitored using a coupled enzyme assay system (32) as previously described with minor modifications (19). Briefly, ATP or GTP (Roche) was added to a final concentration of 1 mM in 100 μl containing: 50 mM Tris-HCl (pH 7.5), 55 mM KCl, 4 mM $MgCl_2$, 1 mM dithiothreitol, 20 units/ml L-lactic dehydrogenase (Sigma), 20 units/ml pyruvate kinase (Sigma), 2 mM phosphoenolpyruvate (Roche), 0.15 mM NADH (Roche), 50 nM UvrA, and 100 nM UvrB (WT or Δ4). Proteins were assayed without DNA (−DNA), or in the presence of 10 ng/μl UV-irradiated DNA (+UV DNA, prepared by exposure of 1 μg/μl pUC18 plasmid DNA to 200 J/m^2 for 1 min) or nondamaged 50-mer ssDNA (+ssDNA, complementary to NDT50). Rate of hydrolysis was calculated from the linear change in absorbance at 340 nm at 55 °C over 30 min, using a Beckman spectrophotometer. Data are reported as the mean rate (M/min) ± S.D. ($n = 3$).

Strand-destabilizing Assay—This assay was done as described previously and the incubations were done at 42 °C (27).

Incision Assays—The 3′-end labeled DNA (2 nM), F50/NDB50 or F50/B8, was incubated with 100 nM UvrB (WT or Δ4) with or without UvrA (20 nM), in 1× ABC buffer (18 μl), at 55 °C for 15 min. After reactions cooled to room temperature, *E. coli* Cho (2 μl, 0.5 μM) was added (37 °C, 30 min). Reactions were terminated with 200 mM EDTA (2 μl), heated to 85 °C (10 min), and cooled on ice. Incision products were resolved on an 18% denaturing polyacrylamide gel (375 V, 50 min, 1× TBE buffer). Gels were processed and developed. Incision products were quantified as described above.

RESULTS

As part of our systematic analysis of the different structural domains of UvrB (10, 19, 27), we chose to further examine domain 4. We constructed a UvrB mutant gene product that has its last 47 amino acid residues (Pro^{612} to Gly^{658}) deleted, UvrBΔ4 (Fig. 1). The last 46 amino acids in *E. coli* UvrB have been shown to form a coiled-coil structure (23,

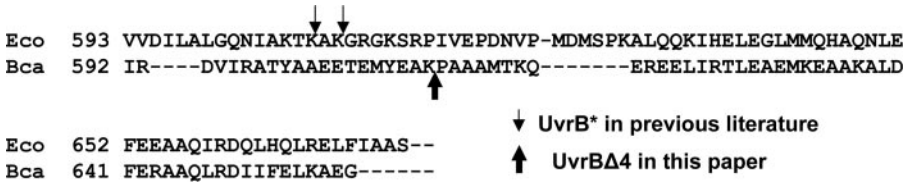

FIGURE 1. **Sequence alignment of C-terminal *E. coli* and *B. caldotenax* UvrB.** Proteolyzed *E. coli* UvrB from cell extracts yielded a 70-kDa fragment (*UvrB**) (39) and mass spectrometric analysis suggested two possibilities for the UvrB* cleavage site(s), between Lys^{607} and Ala^{608} and between Lys^{609} and Gly^{610} (13). *B. caldotenax* UvrBΔ4 has amino acids residues from Pro^{612} to Gly^{658} deleted.

TABLE 1

Estimation of equilibrium dissociation constants of protein dimers

Estimation of the K_d was based on the population of protein dimers (D) and monomers (M) from analysis of their AFM volumes (see Fig. 2). The constants were calculated by the following equation: $K_d = C \times 2(1\text{-}f)^2/f$, in which C is the total protein concentration and $f = 2D/(M + 2D)$.

Protein	Equilibrium dissociation constants (nM) (K_d, mean ± S.D)	Previously reported data
UvrA	3 ± 2	~10 nM
WT UvrB	5 ± 2	NR[a]
UvrBΔ2	4 ± 2	NR
UvrBΔ4	38 ± 8	NR

[a] NR, not reported.

24). We examined the effects of domain 4 truncation on: 1) UvrB self-association; 2) UvrB single-stranded, bubble and duplex DNA binding; 3) UvrB ATPase activity; 4) strand-destabilizing activity of a UvrAB complex; and 5) ability of UvrB to support UvrA-independent incision mediated by Cho.

Equilibrium Dissociation Constants of WT UvrB and UvrBΔ4 Dimer—A key issue in understanding the DNA damage recognition process during NER is the oligomeric state of UvrB. Despite evidence showing that UvrB dimerizes in solution and on DNA (5, 25), we still lack quantitative measurement of the thermodynamic parameters of UvrB self-association and effect of domain 4 truncation on UvrB dimerization. These measurements are prerequisite for understanding the role of UvrB dimer in the NER pathway.

To obtain the equilibrium dissociation constants of WT UvrB and UvrBΔ4 dimers, we took the unique approach of utilizing the protein size information obtained from AFM images. Using topographical AFM images, AFM-derived volumes of proteins have been correlated to their molecular masses, permitting determination of oligomeric states and equilibrium dissociation constants of proteins (29, 30, 33). AFM offers the advantage of assaying proteins with low solubility or with tight binding constants. In addition, sample deposition for AFM imaging can be done over a wide range of temperatures, which is advantageous for studying thermophilic proteins.

Using AFM volume analysis, we found that *B. caldotenax* UvrA dimer has an equilibrium dissociation constant (K_d) of 3 nM (Table 1). These results are consistent with previously published data (K_d at ~10 nM for *E. coli* UvrA) (34). Next, we analyzed WT UvrB. A representative field view AFM image of WT UvrB (20 nM) is shown in Fig. 2*A*. The *inset* is a surface plot of the boxed region (*pink*). The surface plot of WT UvrB clearly shows two distinct populations: proteins with a larger volume (Fig. 2*A*, *green arrows*) and those with a smaller volume (*white arrows*).

Histograms of AFM-derived volumes of WT UvrB are shown in Fig. 2*B*. At 20 nM protein concentration, two distinct peaks are observed at 70 ± 20 and 156 ± 33 nm^3, respectively. Using Equation 1 (see "Materials and Methods"), the peak at 70 nm^3 was calculated to correspond to a ~70-kDa protein, consistent with the size of the UvrB monomer (75 kDa). The peak at 156 nm^3 corresponds to a ~140-kDa protein, consistent with the size of the UvrB dimer (150 kDa). Based on the population of proteins under each peak, the K_d for UvrB dimer is estimated to be 5 nM (Table 1).

The histogram of AFM-derived volumes for UvrBΔ4 (20 nM) also displays two distinct peaks similar to WT UvrB, but located at 89 ± 21 and 175 ± 33 nm^3 (Fig. 2*C*). These volumes correspond to protein molecular masses of ~86 and ~158 kDa, respectively, and are within error of the expected protein size for UvrBΔ4 monomer (65 kDa) and dimer (130 kDa). Compared with the number of protein dimers observed for WT UvrB (217 of 390, 56%), the number of UvrBΔ4 protein dimers observed is almost 50% less (126 of 390, 32%). The K_d for UvrBΔ4 dimer is estimated to be 38 nM (Table 1), ~8-fold higher than WT UvrB.

As a negative control, we imaged the domain 2 deletion mutant of UvrB, UvrBΔ2. Domain 2 of UvrB is believed to interact with UvrA and is not known to play any role in UvrB self-association (19). The histogram of AFM-derived volumes of UvrBΔ2 (20 nM) also displays two distinct peaks (located at 50 ± 20 and 120 ± 30 nm^3, Fig. 2*D*), which correspond to protein molecular masses of ~54 and ~112 kDa, respectively, and are close to that expected for the UvrBΔ2 monomer (60 kDa) and dimer (120 kDa). The K_d for UvrBΔ2 dimer is estimated to be 4 nM (Table 1). Comparing the K_d values of WT, Δ2, and Δ4 UvrB dimers (Table 1) indicates that loss of C-terminal domain 4 significantly alters UvrB monomer-dimer equilibrium, whereas deletion of domain 2 does not have a detectable effect.

DNA Binding Affinity of WT UvrB and UvrBΔ4 Measured by EMSA—Because UvrB has a higher affinity for ssDNA than for duplex DNA (14), we first examined ssDNA binding using EMSA to quantitatively compare the DNA binding affinity of WT UvrB and UvrBΔ4. The nondamaged ssDNA substrate used for this assay was a 50-mer, NDT50 (Fig. 3*A*). The damaged ssDNA substrate, F50, has a fluorescein adduct attached to a centrally located thymine (Fig. 3*A*). Representative EMSA gels are shown in Fig. 4*A*. We observed that UvrBΔ4 has greater affinity for ssDNA than WT UvrB. For example, at 1.5 μM WT UvrB, only 48% of F50 is bound (Fig. 4*A*, *lane 3*). Conversely, at the same protein concentration, close to 90% of F50 is bound by UvrBΔ4 (Fig. 4*A*, *lane 11*).

Notably, two populations of UvrB-DNA complexes are observed via EMSA (faster and slower migrating complexes are labeled *B1-DNA* and *B2-DNA*, respectively, in Fig. 4*A*). These two bands are observed for both WT UvrB and UvrBΔ4. The percentages of B1- and B2-DNA complexes *versus* total protein concentrations are plotted in Fig. 4*A* (*bottom panel*). For WT, at higher protein concentrations (>1 μM), the majority of the protein-DNA complexes are B2-DNA (Fig. 4*A*). For UvrBΔ4, the majority of the complexes are B1-DNA. Given our observation of the effect of domain 4 on UvrB dimerization (Fig. 2), we interpret the B1- and B2-DNA complexes as protein monomer- and dimer-DNA complexes, respectively. Because the percentages of WT B1-DNA or Δ4 B2-DNA are low (<25%), we assume WT UvrB binds DNA primarily as a dimer, whereas UvrBΔ4 binds DNA primarily as a monomer, and calculate the apparent dissociation constants ($K_{d(app)}$) of each complex respectively. Furthermore, in our EMSA, the proteins were in large excess

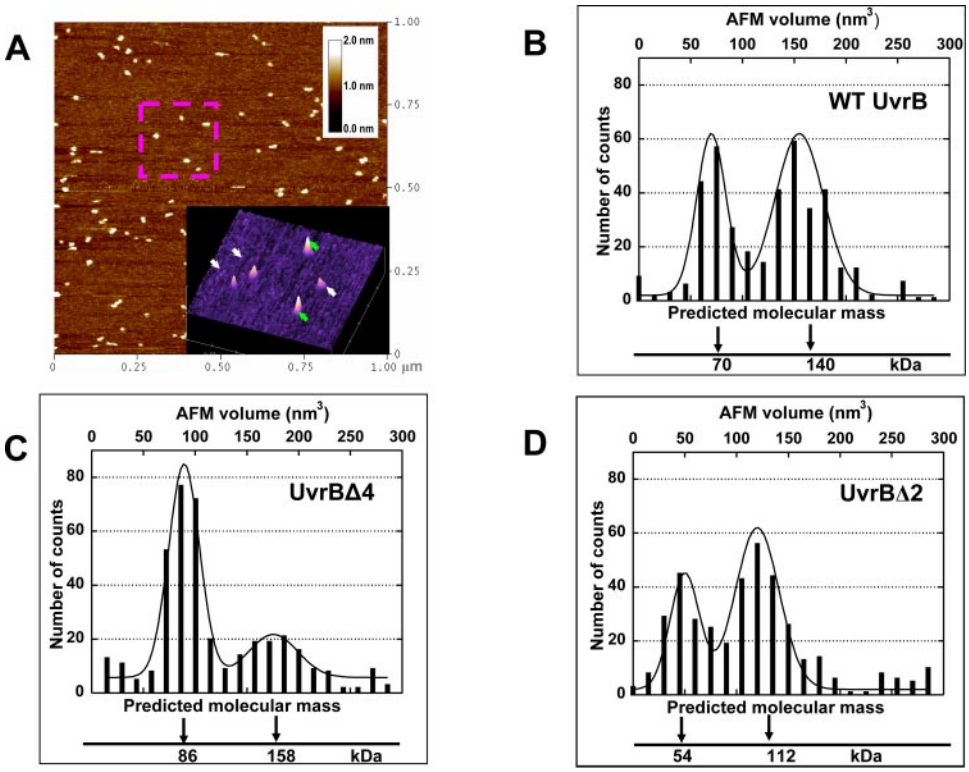

FIGURE 2. **AFM image of UvrB and AFM volume analysis of WT UvrB, UvrBΔ4, and UvrBΔ2.** *A*, a representative field view image of WT UvrB at 20 nM concentration. The actual image size is 1 × 1 μm. The *color bar* represents 0–2 nm height above the mica surface. The *inset* is a surface plot of the *boxed* region (*pink*). *White* and *green arrows* denote UvrB monomers and dimers, respectively. *B–D*, AFM volume analysis of WT UvrB, UvrBΔ4, and UvrBΔ2. The volume of each protein observed from the AFM image was obtained as described under "Materials and Methods." The total data points for each histogram are 390. The *solid lines* are the double Gaussian fits to the data. The *R* value for each curve fit is greater than 0.93. The predicted molecular mass of proteins from the AFM-derived volume was based on Equation 1 under "Materials and Methods."

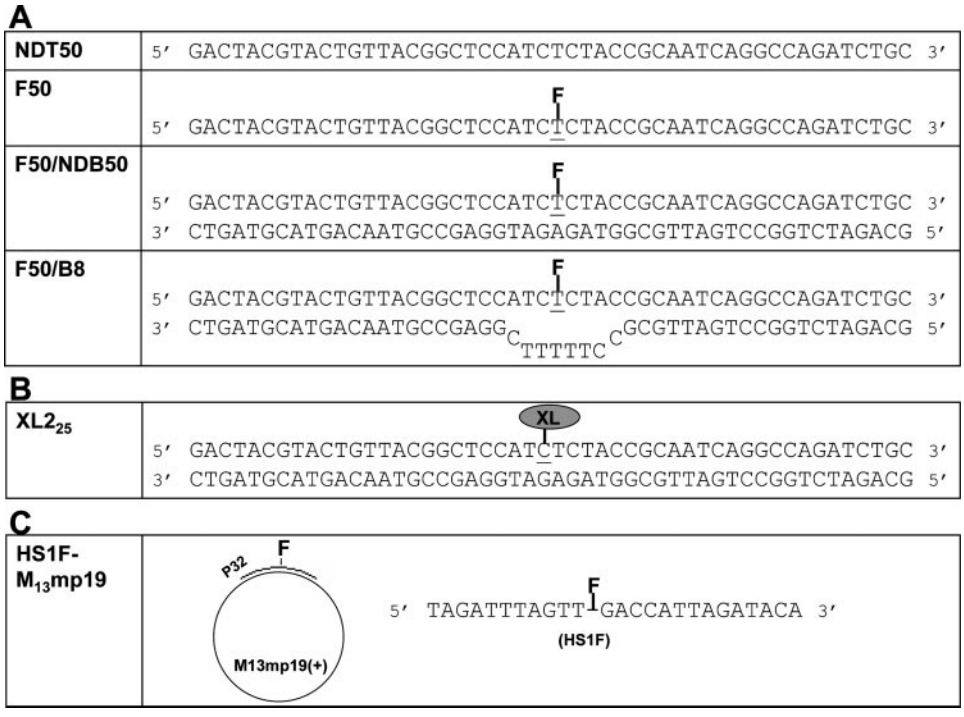

FIGURE 3. **DNA substrates used in this study.** *A*, the DNA substrates used for EMSAs and incision assays. *B*, DNA substrate, $XL2_{25}$ used for photoaffinity cross-linking studies. *XL* in the *gray oval* denotes a photoreactive arylazido group covalently attached to the N4 position of cytosine (10). There is a DNA nick 3′ to the cross-linker. *C*, DNA substrate used for strand-destabilizing assay.

compared with DNA substrates, consequently DNA was not expected to significantly affect the monomer-dimer equilibrium of proteins. Based on this assumption, the concentration of WT dimer and Δ4 monomer present in each reaction was calculated using the equilibrium dissociation constants of protein dimers derived from AFM images (Table 1). To derive $K_{d(app)}$, calculated protein dimer and monomer concentrations were plotted against the percentage of WT B2-DNA and Δ4 B1-DNA complexes, respectively (Fig. 4, *B* and *C*). Based on this analysis, WT UvrB dimer has a $K_{d(app)}$ of 1300 nM on F50 and 2000 nM on NDT50 (Table 2), indicating that WT UvrB has a low specificity for damaged DNA. This is consistent with previous observations that UvrB has weak specificity for some DNA adducts on ssDNA (14, 35). UvrBΔ4 monomer has a $K_{d(app)}$ of 90 nM for F50 and NDT50 (Table 2). These binding constants are 14- and 22-fold tighter than those for WT dimer binding to damaged and nondamaged ssDNA, respectively. These data demonstrate that UvrBΔ4 as a monomer has increased affinity for damaged and nondamaged ssDNA than WT UvrB as a dimer. In contrast to the UvrBΔ4 mutant,

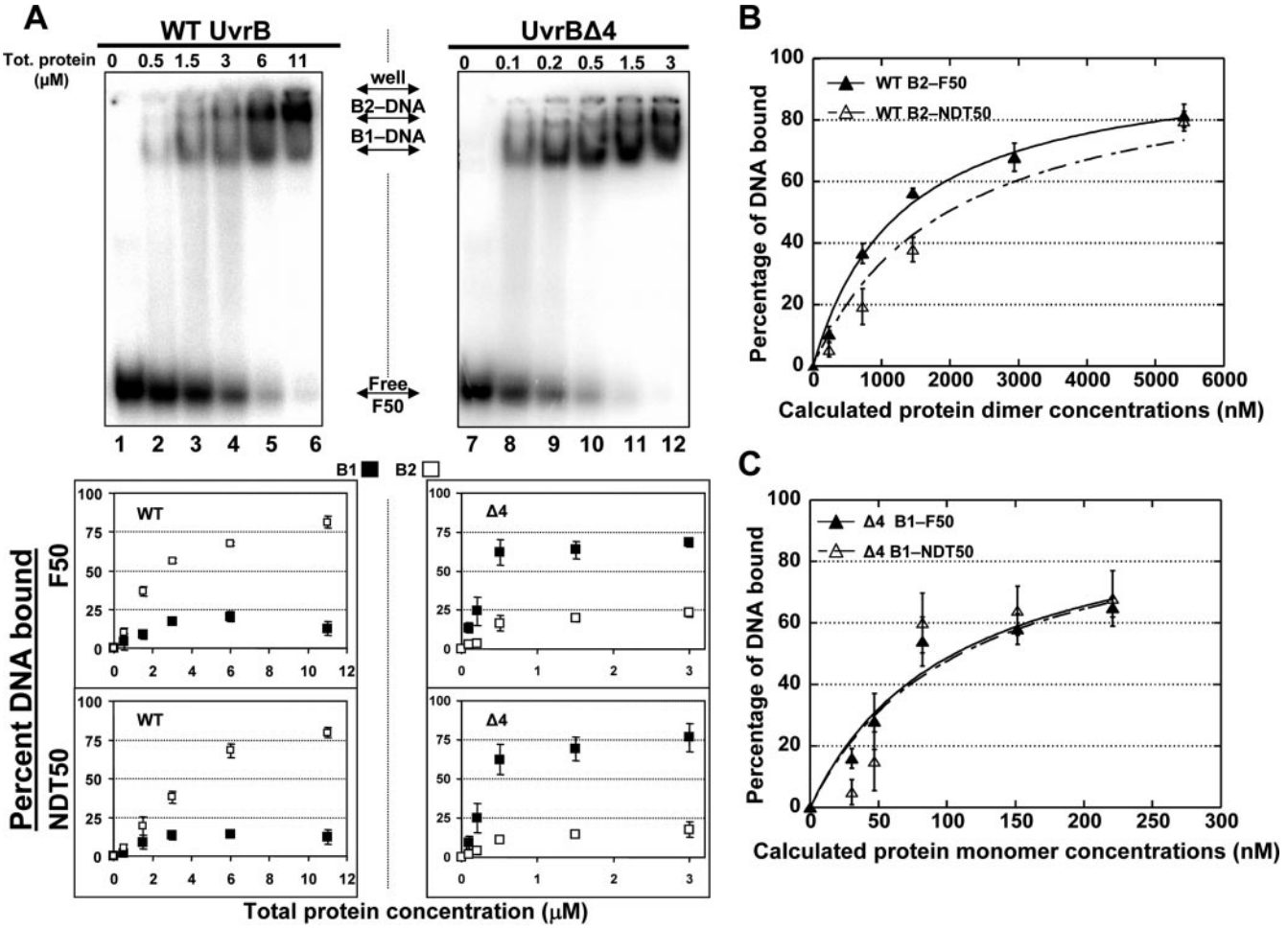

FIGURE 4. **DNA binding affinity of WT UvrB and UvrBΔ4 for ssDNA.** *A*, *top panel*, EMSAs comparing the binding of WT UvrB and UvrBΔ4 to F50 ssDNA (1 nM). The reactions were done in buffer without ATP; *bottom panel*, quantification of WT and Δ4 B1- (*black squares*) and B2-DNA (*white squares*) complexes on F50 and NDT50 substrates. *B* and *C*, calculation of apparent dissociation constants of WT B2-DNA and Δ4 B1-DNA complexes. The derivation of protein dimer and monomer concentrations is described in Table 2. The data plotted were the results from three independent EMSA experiments. The *lines* in the plots are the curve fitting by using nonlinear regression analysis for WT B2-DNA and Δ4 B1-DNA complexes (31). For the curve fitting, R^2 values are ~0.96 and 0.87 for WT and Δ4 data, respectively. The sigmoidal shape of the Δ4 data is because of the loss of the DNA counts in the smear (not counted as protein-DNA complex) at lower protein concentrations.

TABLE 2

Apparent dissociation constants of WT UvrB- and UvrBΔ4-ssDNA complexes

The concentration of WT UvrB dimer and UvrBΔ4 monomer in each reaction was determined using the following equations: $[B_2] = (4 \times [P_{tot}] + K_d - (8 \times [P_{tot}] \times K_d + K_d^2)^{1/2})/8$; $[B_1] = ((K_d^2 + 8 \times K_d \times [P_{tot}])^{1/2} - K_d)/4$; whereas $[B_1]$, $[B_2]$, $[P_{tot}]$ are the monomer, dimer, total protein concentration, respectively; K_d is the equilibrium dissociation constant of protein dimer obtained from AFM images (Table I). Data from EMSA were analyzed as percentage of WT B2-DNA and Δ4 B1-DNA complexes *versus* calculated WT dimer and Δ4 monomer concentration, respectively, and were fitted by nonlinear regression analysis to the equation: $F_b = ((1 + K_aP + K_aD) - ((1 + K_aP + K_aD)^2 - (4DK_a^2P))^{1/2})/2D_TK_a$; whereas P is the protein concentration (calculated dimer for WT and monomer for Δ4); D is the total DNA concentration; $K_a = 1/K_{d(app)}$; $K_{d(app)}$ is the apparent dissociation constant (Schofield *et al.* (31)). The mean ± S.D was derived from three independent experiments.

Protein-DNA complexes	Apparent dissociation constants ($K_{d(app)}$) (mean ± S.D.)	
	Nondamaged ssDNA (NDT50)	Damaged ssDNA (F50)
	nM	
WT UvrB *B2-DNA*	2000 ± 180	1300 ± 50
UvrBΔ4 *B1-DNA*	90 ± 24	90 ± 10

UvrBΔ2 exhibited a lower affinity for ssDNA than WT UvrB (data not shown), indicating that the increased affinity for ssDNA is specifically a result of truncation of domain 4.

It has been shown that *E. coli* UvrB by itself is capable of binding to the sites of lesions embedded in a bubble region or located close to the end of a dsDNA fragment (21, 36, 37). These UvrB-DNA complexes, formed independently of UvrA, also were capable of recruiting UvrC for incisions (21, 36, 37). EMSAs were carried out to investigate whether or not UvrBΔ4 has higher affinity for bubble DNA substrate (F50/B8, sequence shown in Fig. 3*A*). The results are shown in Fig. 5. For WT UvrB, there appears to be two populations of protein-DNA complexes, B1 and B2: faster and slower migrating complexes, respectively; whereas for UvrBΔ4, there is only one predominant population, B1. Overall, both WT and Δ4 have lower affinity for bubble DNA than for ssDNA (compare Fig. 5 with 4). Importantly, consistent with results on ssDNA, UvrBΔ4 has higher affinity for bubble DNA substrate than WT protein. Specifically, at 1.5 μM total protein concentration, only ~6% DNA was bound by WT protein (Fig. 5, *lane 2*); whereas, ~28% DNA was bound by UvrBΔ4 (Fig. 5, *lane 7*).

The Effect of Nucleotide Cofactors on dsDNA Binding of WT UvrB and UvrBΔ4—It is known that the affinity of WT UvrB for fully duplexed dsDNA is very low, therefore we used photoaffinity cross-linking to capture transient interactions between UvrB and dsDNA and study the effect of nucleotide cofactors, namely ATP, GTP, and AMPPNP, on the DNA binding affinity of WT UvrB and UvrBΔ4. Our laboratory previously demonstrated that DNA containing arylazido nucleotide analogs

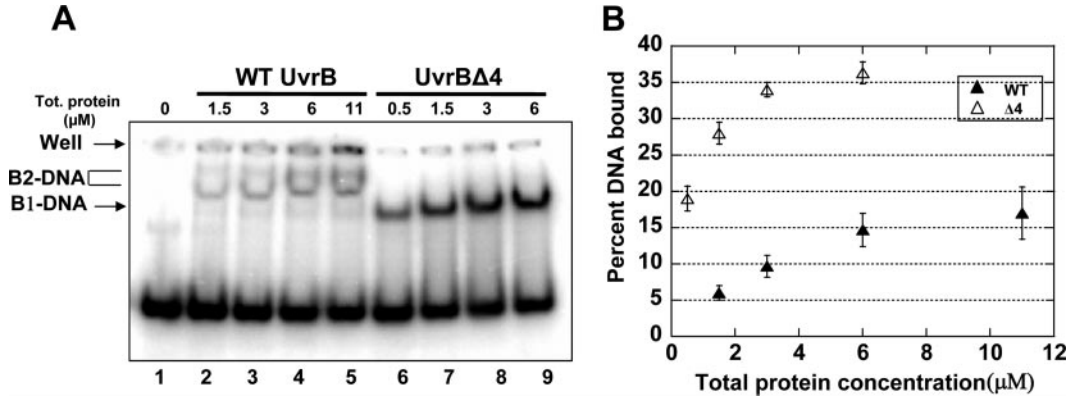

FIGURE 5. **DNA binding affinity of WT UvrB and UvrBΔ4 for bubble DNA.** *A*, electrophoresis mobility shift assay comparing the binding of WT UvrB and UvrBΔ4 to F50/B8 (1 nM). The reactions were done in buffer containing 1 mM ATP. *B*, quantification of binding of WT- and Δ4-DNA complexes to F50/B8. The data plotted were the results from three independent EMSA experiments.

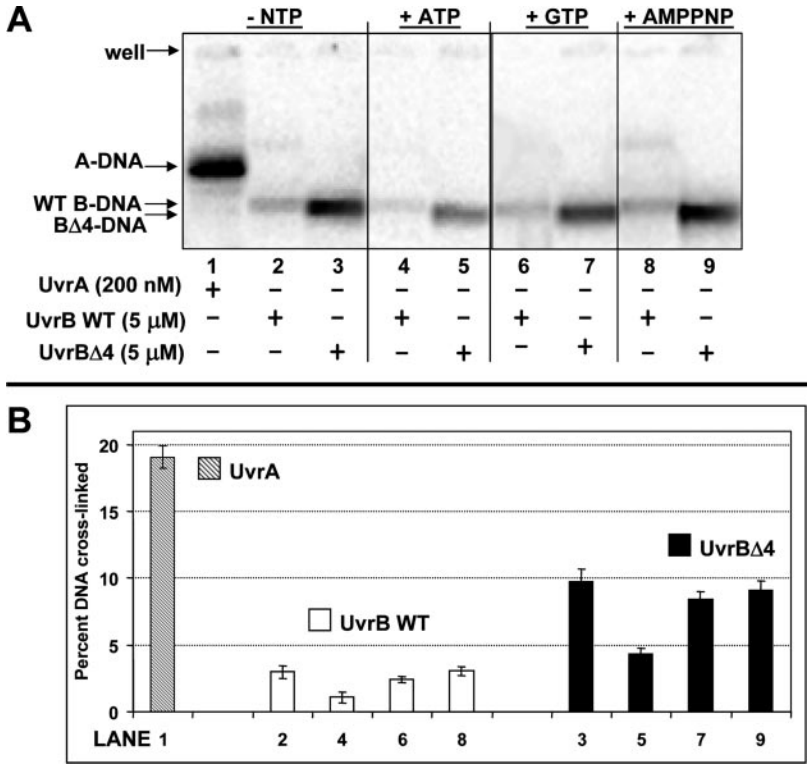

FIGURE 6. **DNA binding of WT UvrB or UvrBΔ4 in the presence of different nucleotide cofactors.** *A*, DNA substrate $XL2_{25}$ (2 nM) was incubated with the indicated protein for 30 min at 55 °C in the dark. Samples were exposed to 5 min of UV (365 nm) and processed as described under "Materials and Methods." *B*, percentage of DNA cross-linked to each protein (n = 3, mean ± S.D.): UvrA (*hatched bar*), WT UvrB (*white bars*), and UvrBΔ4 (*black bars*).

can be used to capture UvrA- and UvrB- DNA complexes by UV-induced cross-linking (10). In this study, the DNA substrate used for cross-linking is $XL2_{25}$ (Fig. 3*B*). A photoreactive cytosine analog with a terminal arylazido group at the N4 position was incorporated into this substrate, and serves as both the site of DNA damage and the cross-linking reagent (10). In these experiments, UvrA (200 nM) was used as a positive control to monitor the efficiency of the cross-linking (Fig. 6, *lane 1*). Representative gels of the samples after cross-linking are shown in Fig. 6*A*, and the extent of cross-linking is summarized in Fig. 6*B*. Results from photoaffinity cross-linking show that in all cases (−NTP, +ATP, +GTP, or +AMPPNP), the amount of UvrBΔ4 cross-linked to $XL2_{25}$ DNA is ~2–3-fold higher than that of WT UvrB (Fig. 6, *lanes 3 versus 2*, *5 versus 4*, *7 versus 6*, and *9 versus 8*).

In addition, we evaluated whether or not domain 4 affects UvrA-dependent loading of UvrB onto damaged duplex DNA. Using EMSA, we found that the rate of UvrA-dependent binding of UvrBΔ4 to dsDNA is slightly faster than WT UvrB, whereas the extent of binding over time is similar (data not shown). Our results are consistent with previous observations that UvrA-dependent loading of a domain 4 truncation mutant of *E. coli* UvrB (UvrB630) is comparable with wild type (38). In summary, the observed DNA binding by UvrBΔ4 itself was significantly greater than that of WT UvrB; however, this difference is diminished for UvrA-dependent loading of UvrB onto damaged DNA.

ATPase Activities of WT UvrB and UvrBΔ4—It has been shown previously that proteolyzed *E. coli* UvrB from cell extracts, UvrB* (Fig. 1), possesses a ssDNA-dependent ATPase activity (39). However, there is no direct comparison between the ATPase activity of WT UvrB and UvrB* in the absence of DNA. To address this question, we used an ATPase assay that is based on a coupled enzyme system to link the hydrolysis of ATP to the oxidation of NADH (32). We found that in the absence of DNA, truncation of domain 4 increases the basal level of ATPase activity of UvrB 9-fold (Fig. 7, *column 4 versus 7*, 2.3×10^{-7} M/min to 2.1×10^{-6} M/min). We observed that nondamaged ssDNA increased ATPase activity of UvrBΔ4 9-fold compared with the basal level (Fig. 7, *column*

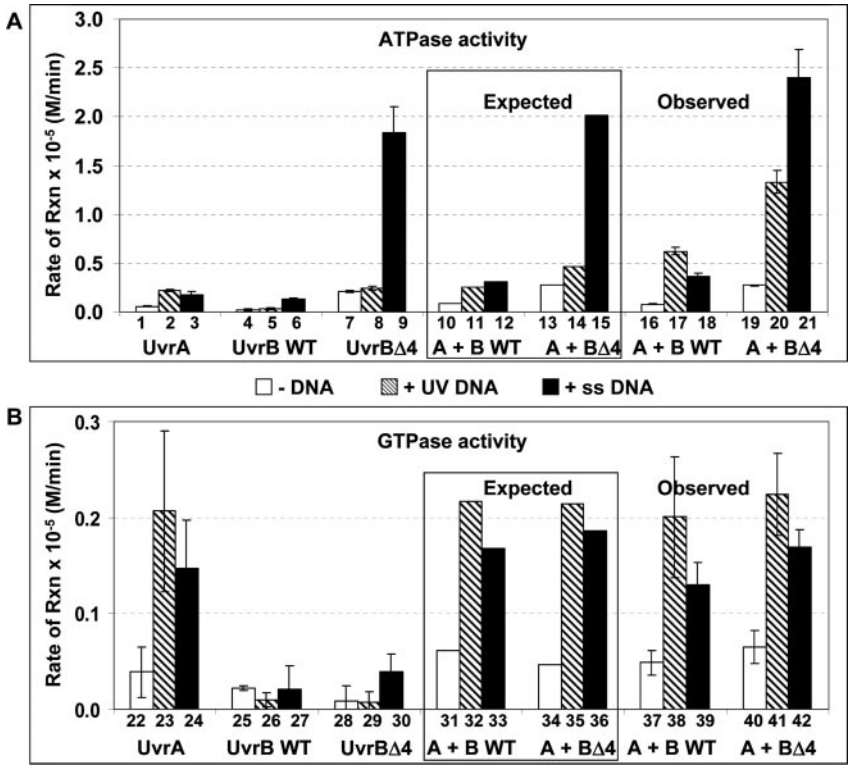

FIGURE 7. **The ATPase and GTPase activity of WT UvrB and UvrBΔ4.** Both WT UvrB and UvrBΔ4 were assayed for their ATPase (*A*) and GTPase (*B*) activities individually and in the presence of UvrA at 55 °C. The DNA substrate in the reaction was also varied: −DNA (*white bars*), +UV irradiated DNA plasmid (*hatched bars*), and +nondamaged ssDNA (*black bars*). The columns labeled *Expected* and *Observed* are the values of the sum of the ATPase activities of individual proteins and the values measured when mixing two proteins together, respectively. $n = 3$, mean ± S.D.

9 versus 7), and only increased ATPase activity of WT UvrB 5-fold (Fig. 7, *column 6 versus 4*), which is consistent with previous results (39). Overall, in the presence of 50-mer ssDNA, UvrBΔ4 has 14-fold higher ATPase activity than WT UvrB (Fig. 7, *column 9 versus 6*). UV-irradiated plasmid DNA (in the absence of UvrA) had no significant effect on the ATPase activity of either WT UvrB or UvrBΔ4 (Fig. 7, for WT, *column 4 versus 5*; for Δ4, *column 7 versus 8*), indicating that interaction with ssDNA is essential to activate the ATPase of UvrB.

Next, we examined the effect of domain 4 truncation on ATPase activity of the UvrAB complex. In the absence of DNA, the ATPase activity of UvrAB or UvrABΔ4 complexes is essentially the sum of the ATPase activity of the individual proteins (Fig. 7, *column 10 versus 16* and *13 versus 19*). However, in the presence of UV-irradiated plasmid DNA, the ATPase activity of the UvrAB complex is 2.4-fold higher than the sum of individual protein activity (Fig. 7, *column 17 versus 11*), and 2.8-fold higher in the case of UvrABΔ4 complex (Fig. 7, *column 20 versus 14*). These data indicate that in the presence of damaged dsDNA, the ATPase activity of UvrAB and UvrABΔ4 are stimulated to the same extent. In addition, these data suggest that in the presence of nondamaged ssDNA, there is no further stimulation of ATPase activity of UvrAB or UvrABΔ4 complex (Fig. 7, *column 18 versus 12*, *21 versus 15*).

The following question remains: is the stimulated ATPase activity of UvrAB and UvrABΔ4 complex in the presence of UV-irradiated plasmid due to further activation of the ATPase activity of UvrA or unmasking the ATPase activity of UvrB/UvrBΔ4? To answer this question, a GTPase assay was performed to distinguish the activity contributed by each protein in the UvrAB complex. This experiment is based on the knowledge that UvrA can hydrolyze both ATP and GTP, but UvrB can only hydrolyze ATP (40). A summary of the GTPase assay results is shown in Fig. 7*B*. The presence of UV-irradiated plasmid or nondamaged ssDNA stimulated the GTPase activity of UvrA (Fig. 7, *columns 23* and *24 versus 22*). However, addition of either WT UvrB or UvrBΔ4 does not stimulate the GTPase activity of UvrA further (Fig. 7, *columns 32 versus 38*, *33 versus 39*, *35 versus 41*, and *36 versus 42*). These results support the notion that when UvrA and UvrB are combined together in the presence of damaged DNA, the stimulated ATPase activity above the sum of the individual protein activity is because of the DNA damage-dependent unlocking of the ATPase activity of UvrB by UvrA. Taken together, these data (Fig. 7, *A* and *B*) demonstrated that truncation of domain 4 increases: 1) the basal ATPase level; 2) ssDNA-dependent ATPase activity; and 3) UvrA- and DNA damage-dependent ATPase activity of UvrB.

Strand-destabilizing Activity of WT UvrAB and UvrABΔ4—The limited strand opening activity by the UvrAB complex is believed to be important in opening up the hydrophobic interior of DNA to allow appropriate positioning of UvrB for damage recognition (21, 41). This strand-destabilizing activity can be monitored by an assay that measures the release of radioactively labeled oligonucleotide (<27-mer) annealed to circular ssDNA (41, 42). It is worth noting that the UvrAB complex only destabilizes duplex DNA, and oligonucleotide is not released from the circular ssDNA until addition of a stop buffer containing SDS and EDTA. An early report stated that *E. coli* UvrB* was completely defective in the strand-destabilizing assay (43). However, more recently it was reported that UvrAB* complex could support incision mediated by Cho (44). Consequently, we decided to reevaluate whether or not the truncation of domain 4 impairs the strand-destabilizing activity. The DNA substrate used for this assay is shown in Fig. 3*C*. The results from this assay are shown in Fig. 8*A* with kinetics of the 26-mer release summarized in Fig. 8*C*. Contrary to previous results (43), we observed that UvrBΔ4 supported destabilization of the fluorescein-containing 26-mer as efficiently as WT UvrB ($t_{1/2} \approx 16$ min). In addition, the destabilization of small oligos annealed to circular ssDNA by UvrAB and UvrABΔ4 complexes is damage specific, because after a 60-min incubation under the same reaction conditions, less than 15% of a nondamaged 26-mer was released by either UvrAB or UvrABΔ4 complexes (data not shown). Furthermore, there was no detectable strand-destabilizing activity when only UvrB or UvrBΔ4 was present (Fig. 8*B*).

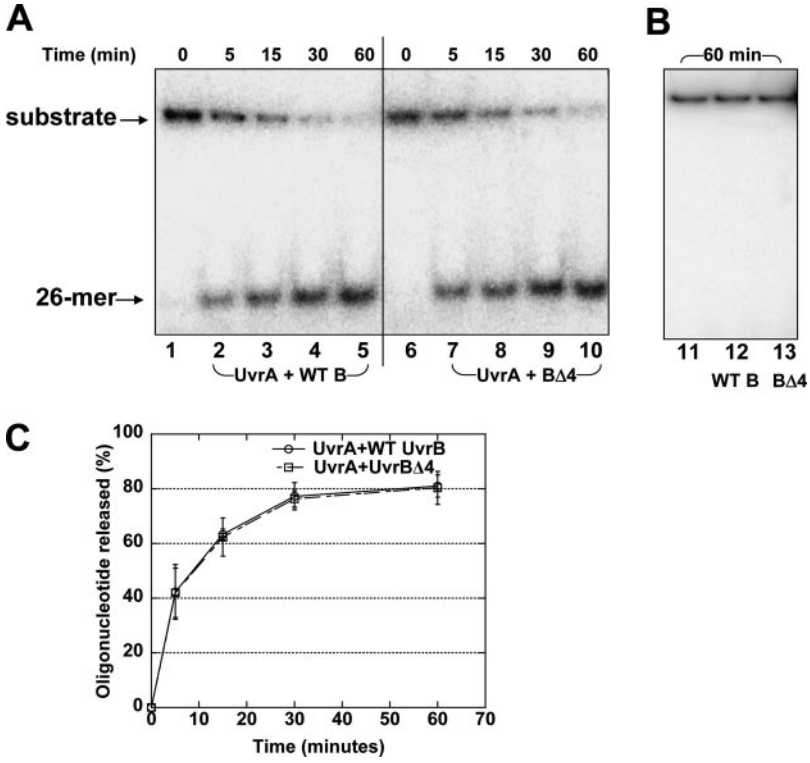

FIGURE 8. **Strand-destabilizing activities of WT UvrB and UvrBΔ4.** *A*, the kinetics of 26-mer release by UvrAB (*lane 1-5*) and UvrABΔ4 (*lane 6-10*) monitored by gel electrophoresis. *B*, monitoring the oligonucleotide release in the presence of only WT UvrB (*lane 12*) or UvrBΔ4 (*lane 13*). *C*, quantitative comparison between the strand-destabilizing activities of WT UvrAB and UvrABΔ4. $n = 3$, mean ± S.D.

WT UvrB and UvrBΔ4 Supported Incision Mediated by Cho—We found that compared with WT UvrB, UvrBΔ4 has higher UvrA-independent affinity for ssDNA, bubble, and duplex DNA (Figs. 4–6). These observations led us to question whether UvrBΔ4 could support more efficient incision than WT UvrB in the absence of UvrA. We used the *E. coli* Cho protein to address this question, because it has been observed that *E. coli* UvrB* (13) and *B. caldotenax* UvrBΔ4 (data not shown) are defective in recruiting UvrC to make the 3′ incision, whereas UvrAB* complex can support incision mediated by Cho (44). Presumably, UvrC and Cho bind to different regions of UvrB. It was reported that Cho can incise DNA at the 3′ side of the damage site and that the incision site of Cho is located four nucleotides further away from the damage compared with the 3′ incision site of *E. coli* UvrC (44).

Initially, we tested the possibility that UvrBΔ4 could support more efficient incision by using a 50-bp duplex substrate, F50/NDB50 (Fig. 3*A*). The results are shown in Fig. 9*A*. We observed two prominent Cho incision products (Fig. 9*A*, labeled *P1* and *P2*). Previously, only one Cho incision product was observed on a 50-bp substrate containing a cholesterol lesion using *E. coli* UvrA and UvrB proteins (44). However, variation of the 3′ incision site has been observed on substrates containing site-specifically modified N2-guanine BPDE adducts (45). Variation of the 3′ incision site has been attributed to the stereochemistry and orientation of the BPDE adduct. Future studies are needed to address whether the presence of two 3′ Cho incision sites is specific to *B. caldotenax* proteins or to the fluorescein containing substrate. For purposes of quantitative analysis, both bands (P1 and P2) were counted as incision products. In the presence of UvrA, WT UvrB and UvrBΔ4 supported incision of 7 and 14% of the F50/NDB50 DNA substrate, respectively (Fig. 9, *lanes 2* and *4*). However, in the absence of UvrA, WT UvrB- and UvrBΔ4-supported incisions were less than 1% of the total DNA substrate (Fig. 9, *lanes 3* and *5*). These data indicate that even though UvrBΔ4 has higher affinity for duplex DNA, formation of the active form of UvrBΔ4-DNA complex on fully duplexed DNA apparently requires UvrA to help facilitate unwinding DNA.

Next, we examined incision on a DNA substrate containing an 8-bp bubble, F50/B8. Under the same experimental conditions, in the presence of UvrA, both WT UvrB and UvrBΔ4 supported more efficient incision of bubble substrate than of the fully duplexed DNA (Fig. 9, *lane 7 versus 2* and *lane 9 versus 4*). In addition, UvrABΔ4 supported incision of F50/B8 with slightly higher efficiency than WT UvrAB (Fig. 9, *lane 9 versus 7*). A dramatic difference is seen on the bubble substrate in the absence of UvrA. In this case, whereas WT UvrB supported little incision of the bubble substrate (~3%, Fig. 9, *lane 8*), UvrBΔ4 supported incision of 41% of the bubble substrate (Fig. 9, *lane 10*). Similar results were observed with a 6-bp bubble (data not shown). It is worth noting that UvrBΔ4 supported incision of the nondamaged bubble DNA substrate mediated by Cho was less than 1% (data not shown). These data imply that loss of domain 4 allows the UvrBΔ4 mutant by itself to load properly onto DNA, and DNA damage is needed to trigger the conformational change in UvrBΔ4 that can lead to incision. In summary, our results clearly show that: 1) the incision efficiency of Cho is higher on bubble substrate than on fully duplexed DNA (Fig. 9, *lane 7 versus 2*); 2) independent of UvrA, UvrBΔ4 supports more efficient incision by Cho on bubble substrate (Fig. 9, *lane 10 versus 8*) than wild type protein.

DISCUSSION

The enhancement of an activity of a particular domain, such as DNA binding or ATPase, in the absence of some other region of the protein indicates autoinhibition (26). The discovery of an autoinhibitory domain is often through the characterization of the activity of fragments of a protein relative to the activity of the full-length protein. The enhancement of an activity of a truncated form of protein indicates existence of an autoinhibitory domain. Autoinhibition is a widespread regulatory strategy in regulation of protein function. In this study, using two different DNA binding assays, namely EMSAs and photoaffinity cross-linking, we made the surprising discovery that domain 4 of UvrB is an autoinhibitory domain (Fig. 10). Specifically, we report that

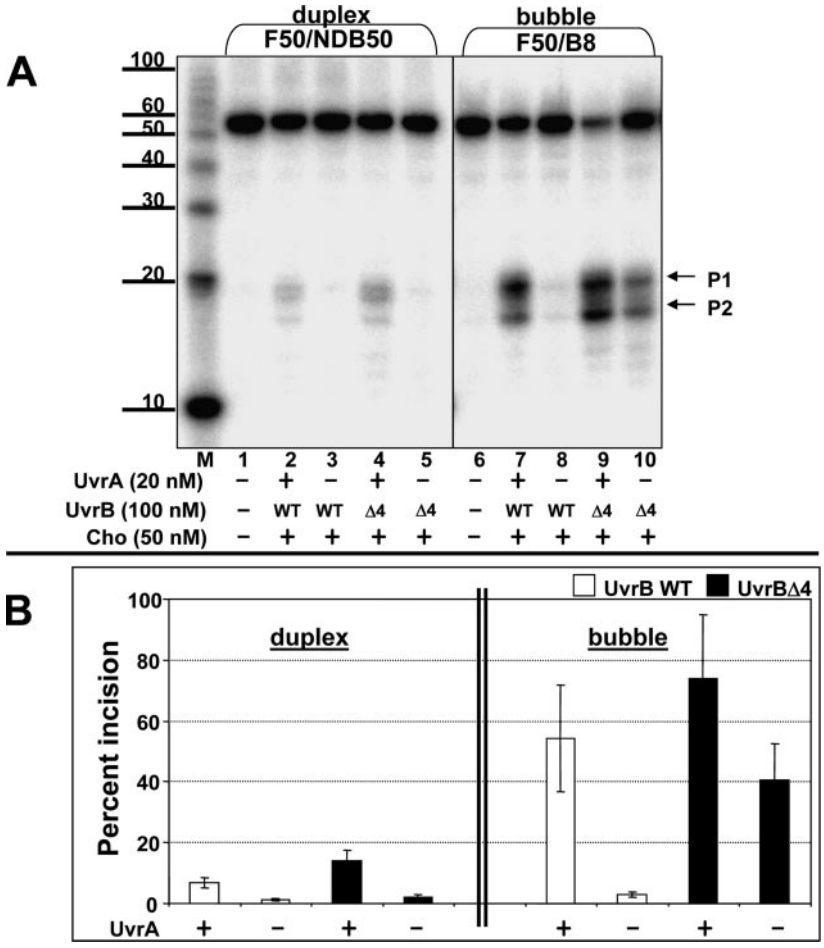

FIGURE 9. **WT UvrB and UvrBΔ4 supported incisions mediated by Cho.** *A*, incisions of F50/NDB50 and F50/B8 substrates. *B*, graphic comparison of incision of F50/NDB50 and F50/B8 substrates mediated by Cho. $n = 3$, mean ± S.D.

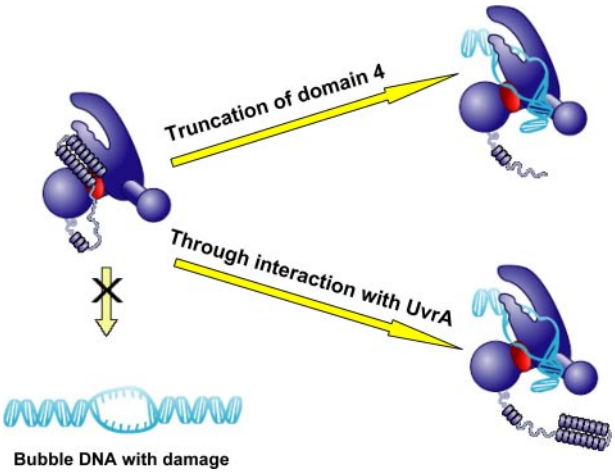

FIGURE 10. **Autoinhibition by domain 4 of UvrB.** The *red circle* on the UvrB model represents the ATP binding site. The enhancement of DNA binding and ATPase activities in the absence of domain 4 indicates autoinhibition (*top right*). We propose that the autoinhibitory effect of domain 4 can be relieved by association with UvrA (*bottom right*), and this hypothesis is graphically demonstrated by showing domain 4 moved away from the rest of the protein. However, defining the mechanism of autoinhibition and understanding how autoinhibition is relieved by UvrA require further investigation.

UvrBΔ4, as a monomer, has a 14- and 22-fold higher binding affinity for damaged and nondamaged ssDNA, respectively, than WT UvrB as a dimer (Fig. 4). In addition, our results demonstrated that this increased DNA binding is independent of nucleotide cofactors (Fig. 6). Domain 4 truncation also has a significant effect on ATPase activity of UvrB: it increases the basal ATPase activity 9-fold and ssDNA-dependent ATPase activity 14-fold (Fig. 7). Consistent with increased DNA binding affinity and ATPase activity, this mutant of UvrB supports more efficient UvrA-independent incision mediated by Cho (Fig. 9).

The idea that domain 4 of UvrB behaves as an autoinhibitory domain is also consistent with a general feature of autoinhibition: the autoinhibitory domains are often linked to the remaining part of the protein by flexible regions (26). The transition from the inhibited to the activated state usually requires this flexibility. For UvrB, the C-terminal coiled-coil region of domain 4 is linked to domain 3 through a flexible linker region 24–72 residues long depending on species (22).

We observed that after truncation of domain 4, the ATPase activity of UvrB was increased 9-fold in the absence of DNA. The ATP binding site of UvrB is located between domains 1a and 3. Based on the structural similarity between UvrB and helicases, it has been suggested that ATP hydrolysis in UvrB is coupled to the motion of domains 1a and 3 that close down on DNA. In helicase superfamily II, two arginines in motif VI are located near the scissile P–P bond during catalysis (16, 22). These residues are believed to participate in polarization of the scissile bond and stabilization of the developing negative charge at the β-phosphate during ATP hydrolysis. In the crystal structure of *B. caldotenax* UvrB, the closest arginines, Arg^{543} and Arg^{540}, are still too distant from the ATP molecule for direct interactions, thus explaining why the nucleotide cannot be hydrolyzed. It is possible that removal of domain 4 might change the conformation of the loop that connects domains 3 and 4 and the adenine binding pocket of UvrB, thus uncoupling ATPase activity and domain movement (22). In the context of intact UvrB, repositioning of domain 4 relative to other domains of UvrB through the interaction between UvrA and UvrB might alter the ATP binding pocket. Results

based on using *E. coli* UvrB mutants that had a tryptophan reporter group at the ATP binding motif suggests that the accessibility of the ATP binding site in WT UvrB is comparable with UvrB* (46). These data also support a model of allosteric regulation of ATP hydrolysis by domain 4 and argue against physical masking of the ATP binding site by domain 4. These ideas are consistent with the recent finding by Barrett and co-workers (47) who have crystallized UvrB bound to oligo(dT)$_3$ in a ternary complex with ATP. In this structure domain 4 was removed by proteolysis during crystallization thus enabling ATP binding.

The common mechanisms for relieving autoinhibition include: displacement of the inhibitory domain by a second protein, proteolysis of the inhibitory domain, and post-translational modification or binding of small molecules that allosterically alter the inhibitory domain (26). If domain 4 is an autoinhibitory domain, it is reasonable to suggest that relieving the inhibition provided by domain 4 of UvrB involves the interaction between UvrB and UvrA. This suggestion is supported by our observation that removal of domain 4 enhanced the direct binding of UvrB to DNA (Figs. 4–6), but UvrA-dependent binding of WT UvrB and UvrBΔ4 to duplex DNA containing damage are similar (data not shown). Previously, Hsu *et al.* (14), using maltose-binding protein fused with residues 547 to 673 from *E. coli* UvrB (containing the coiled-coiled domain), observed that *E. coli* UvrA directly interacts with this part of *E. coli* UvrB. Taking this observation together with our results, we propose that UvrA relieves the inhibitory effect of domain 4 through protein-protein interactions (Fig. 10).

In general, an autoinhibition domain presents a reversible barrier that prevents spurious activation of a biological pathway (26). In other words, an autoinhibition mechanism is a constitutive damper that serves to repress an activity, and only allows it to be executed in the presence of an activation signal that is sufficiently strong to overcome this barrier (26). In the case of the bacterial NER system, the presence of domain 4 as an autoinhibitory domain may be necessary for increasing the damage specificity of UvrB and for UvrB to be primed for recruiting UvrC only through interaction with UvrA. Unregulated direct binding of UvrB to DNA might provoke spurious incision reactions and could present a roadblock to various DNA transaction events, such as DNA replication, recombination, and other DNA repair pathways.

Another key issue in understanding the DNA damage recognition process during NER is the oligomeric state of UvrB. UvrB was proposed to function as a monomer from early gel filtration and sedimentation studies (4). However, evidence has emerged supporting the notion that UvrB can dimerize and it was suggested that dimerization might be essential for alternate scanning of both DNA strands (5, 25). Based on volume analysis of the proteins from AFM images, we estimated that the K_d for WT UvrB dimer is in the lower nanomolar range. Truncation of domain 4 of UvrB weakens the self-dimerization, increasing the K_d from 5 to 38 nM. We also discovered that domain 4 truncation leads to both increased DNA binding and ATPase activity. Furthermore, UvrBΔ4 is more efficient than WT UvrB in supporting UvrA-independent incision of bubble DNA by Cho (Fig. 9). These data suggest that UvrBΔ4 with its ability to dimerize significantly compromised is completely functional, and UvrB monomer could be the catalytically active form of UvrB. It is possible that after initial recognition of DNA damage by UvrA, verification of DNA damage by UvrB involves two steps. First, dimeric UvrB forms a weak complex with DNA. Second, to achieve tight DNA binding to form the preincision UvrB-DNA complex, one UvrB subunit would dissociate. A question that remains is: does UvrA regulate UvrB dimer formation? In an analogous system, it has been demonstrated that TFIIA promotes the dissociation of TATA-box-binding protein (TBP) dimers directly and accelerates the kinetics of DNA binding by TBP (48). Furthermore, domain 4 truncation seems to only destabilize the UvrB dimer, and not totally abolish dimerization (Fig. 2 and Table 1) (5, 25). Most likely, other residues in UvrB also participate in the dimerization and remain to be characterized. In summary, we propose that domain 4 of UvrB acts as an autoinhibitory gate for stepwise regulation of DNA binding, ATPase activity, and protein-protein interactions (Fig. 10).

Acknowledgments—We thank Drs. Leroy Worth, Jr. and William A. Beard for critical reading of this manuscript, Kolappan Subramaniapillai for technical support of purification of Cho, Paul Cacioppo for assistance with graphics, and Dr. Robert Petrovich and Lori Edwards of the NIEHS Protein Core Facility for assistance with production of the proteins.

REFERENCES

1. Van Houten, B. (1990) *Microbiol. Rev.* **54,** 18–51
2. Goosen, N., and Moolenaar, G. F. (2001) *Res. Microbiol.* **152,** 401–409
3. Van Houten, B., Croteau, D. L., DellaVecchia, M. J., Wang, H., and Kisker, C. (2005) *Mutat. Res.* **577,** 92–117
4. Orren, D. K., and Sancar, A. (1989) *Proc. Natl. Acad. Sci. U. S. A.* **86,** 5237–5241
5. Verhoeven, E. E., Wyman, C., Moolenaar, G. F., and Goosen, N. (2002) *EMBO J.* **21,** 4196–4205
6. Kacinski, B. M., and Rupp, W. D. (1981) *Nature* **294,** 480–481
7. Bertrand-Burggraf, E., Selby, C. P., Hearst, J. E., and Sancar, A. (1991) *J. Mol. Biol.* **219,** 27–36
8. Shi, Q., Thresher, R., Sancar, A., and Griffith, J. (1992) *J. Mol. Biol.* **226,** 425–432
9. Verhoeven, E. E., Wyman, C., Moolenaar, G. F., Hoeijmakers, J. H., and Goosen, N. (2001) *EMBO J.* **20,** 601–611
10. DellaVecchia, M. J., Croteau, D. L., Skorvaga, M., Dezhurov, S. V., Lavrik, O. I., and Van Houten, B. (2004) *J. Biol. Chem.* **279,** 45245–45256
11. Sancar, A., and Rupp, W. D. (1983) *Cell* **33,** 249–260
12. Yeung, A. T., Mattes, W. B., Oh, E. Y., and Grossman, L. (1983) *Proc. Natl. Acad. Sci. U. S. A.* **80,** 6157–6161
13. Moolenaar, G. F., Franken, K. L., Dijkstra, D. M., Thomas-Oates, J. E., Visse, R., van de Putte, P., and Goosen, N. (1995) *J. Biol. Chem.* **270,** 30508–30515
14. Hsu, D. S., Kim, S. T., Sun, Q., and Sancar, A. (1995) *J. Biol. Chem.* **270,** 8319–8327
15. Gorbalenya, A. E., Koonin, E. V., Donchenko, A. P., and Blinov, V. M. (1989) *Nucleic Acids Res.* **17,** 4713–4730
16. Theis, K., Chen, P. J., Skorvaga, M., Van Houten, B., and Kisker, C. (1999) *EMBO J.* **18,** 6899–6907
17. Machius, M., Henry, L., Palnitkar, M., and Deisenhofer, J. (1999) *Proc. Natl. Acad. Sci. U. S. A.* **96,** 11717–11722
18. Nakagawa, N., Sugahara, M., Masui, R., Kato, R., Fukuyama, K., and Kuramitsu, S. (1999) *J. Biochem.* (*Tokyo*) **126,** 986–990
19. Truglio, J. J., Croteau, D. L., Skorvaga, M., DellaVecchia, M. J., Theis, K., Mandavilli, B. S., Van Houten, B., and Kisker, C. (2004) *EMBO J.* **23,** 2498–2509
20. Gordienko, I., and Rupp, W. D. (1997) *EMBO J.* **16,** 880–888
21. Zou, Y., and Van Houten, B. (1999) *EMBO J.* **18,** 4889–4901
22. Theis, K., Skorvaga, M., Machius, M., Nakagawa, N., Van Houten, B., and Kisker, C. (2000) *Mutat. Res.* **460,** 277–300
23. Sohi, M., Alexandrovich, A., Moolenaar, G., Visse, R., Goosen, N., Vernede, X., Fontecilla-Camps, J. C., Champness, J., and Sanderson, M. R. (2000) *FEBS Lett.* **465,** 161–164
24. Alexandrovich, A., Czisch, M., Frenkiel, T. A., Kelly, G. P., Goosen, N., Moolenaar, G. F., Chowdhry, B. Z., Sanderson, M. R., and Lane, A. N. (2001) *J. Biomol. Struct. Dyn.* **19,** 219–236
25. Hildebrand, E. L., and Grossman, L. (1999) *J. Biol. Chem.* **274,** 27885–27890
26. Pufall, M. A., and Graves, B. J. (2002) *Annu. Rev. Cell Dev. Biol.* **18,** 421–462
27. Skorvaga, M., Theis, K., Mandavilli, B. S., Kisker, C., and Van Houten, B. (2002) *J. Biol. Chem.* **277,** 1553–1559
28. Wang, H., Yang, Y., Schofield, M. J., Du, C., Fridman, Y., Lee, S. D., Larson, E. D., Drummond, J. T., Alani, E., Hsieh, P., and Erie, D. A. (2003) *Proc. Natl. Acad. Sci. U. S. A.* **100,** 14822–14827
29. Ratcliff, G. C., and Erie, D. A. (2001) *J. Am. Chem. Soc.* **123,** 5632–5635
30. Yang, Y., Wang, H., and Erie, D. A. (2003) *Methods* **29,** 175–187
31. Schofield, M. J., Lilley, D. M., and White, M. F. (1998) *Biochemistry* **37,** 7733–7740
32. Panuska, J. R., and Goldthwait, D. A. (1980) *J. Biol. Chem.* **255,** 5208–5214
33. Wyman, C., Rombel, I., North, A. K., Bustamante, C., and Kustu, S. (1997) *Science* **275,** 1658–1661
34. Myles, G. M., Hearst, J. E., and Sancar, A. (1991) *Biochemistry* **30,** 3824–3834
35. Yamagata, A., Masui, R., Kato, R., Nakagawa, N., Ozaki, H., Sawai, H., Kuramitsu, S., and Fukuyama, K. (2000) *J. Biol. Chem.* **275,** 13235–13242
36. Zou, Y., Walker, R., Bassett, H., Geacintov, N. E., and Van Houten, B. (1997) *J. Biol.*

Chem. **272,** 4820–4827
37. Moolenaar, G. F., Monaco, V., van der Marel, G. A., van Boom, J. H., Visse, R., and Goosen, N. (2000) *J. Biol. Chem.* **275,** 8038–8043
38. Malta, E., Moolenaar, G. F., and Goosen, N. (2006) *J. Biol. Chem.* **281,** 2184–2194
39. Caron, P. R., and Grossman, L. (1988) *Nucleic Acids Res.* **16,** 10891–10902
40. Thiagalingam, S., and Grossman, L. (1993) *J. Biol. Chem.* **268,** 18382–18389
41. Gordienko, I., and Rupp, W. D. (1997) *EMBO J.* **16,** 889–895
42. Oh, E. Y., and Grossman, L. (1987) *Proc. Natl. Acad. Sci. U. S. A.* **84,** 3638–3642
43. Caron, P. R., and Grossman, L. (1988) *Nucleic Acids Res.* **16,** 10903–10912
44. Moolenaar, G. F., van Rossum-Fikkert, S., van Kesteren, M., and Goosen, N. (2002) *Proc. Natl. Acad. Sci. U. S. A.* **99,** 1467–1472
45. Zou, Y., Liu, T. M., Geacintov, N. E., and Van Houten, B. (1995) *Biochemistry* **34,** 13582–13593
46. Hildebrand, E. L., and Grossman, L. (1998) *J. Biol. Chem.* **273,** 7818–7827
47. Eryilmaz, J., Ceschini, S., Ryan, J., Geddes, S., Waters, T. R., and Barrett, T. E. (2006) *J. Mol. Biol.* **357,** 62–72
48. Coleman, R. A., Taggart, A. K., Burma, S., Chicca, J. J., 2nd, and Pugh, B. F. (1999) *Mol. Cell* **4,** 451–457
49. Truglio, J. J., Karakas, E., Rhau, B., Wang, H., Della Vecchia, M. J., Van Houten, B., and Kisker, C. (2006) *Nat. Struct. Mol. Biol.* **13,** 360–364